



Article

# New O- and N-N-Bridging Complexes of Tc(V), the Role of the Nitrogen Atom Position in Aromatic Rings: Reaction Mechanism, Spectroscopy, DTA, XRD and Hirshfeld Surface Analysis

Anton Petrovich Novikov <sup>\*</sup> and Mikhail Alexandrovich Volkov

Frumkin Institute of Physical Chemistry and Electrochemistry, Russian Academy of Sciences,  
Leninskii Prospect 31-4, 119071 Moscow, Russia

\* Correspondence: tony.novickoff@yandex.ru

**Abstract:** In this work, O- and N-N-bridging complexes of technetium (V), previously known only for rhenium, were obtained for the first time. Tc(V) complexes with pyridazine (pyd), 1,2,4-triazole (trz), 3,5-dimethylpyrazole (dmpz) and pyrimidine (pyr) were obtained. In three complexes  $[\{\text{TcOCl}_2\}_2(\mu\text{-O})(\mu\text{-pyd})_2]$ ,  $[\{\text{TcOCl}_2\}_2(\mu\text{-O})(\mu\text{-trz})_2]\cdot\text{Htrz}\cdot\text{Cl}$  and  $[\{\text{TcO}(\text{dmpz})_4\}(\mu\text{-O})(\text{TcOCl}_4)]$  two technetium atoms are linked by a Tc-O-Tc bond, and in the first two, Tc atoms are additionally linked by a Tc-N-N-Tc bond through the nitrogen atoms of the aromatic rings. We determined the role of nitrogen atom position in the aromatic ring and the presence of substituents on the formation of such complexes. For the first time, a reaction mechanism for the formation of such complexes was proposed. This article details the crystal structures of four new compounds. The work describes in detail the coordination of Tc atoms in the obtained structures and the regularities of the formation of crystal packings. The spectroscopic properties of the obtained compounds and their mother solutions were studied. The decomposition temperatures of the described complexes were determined. An assumption was made about the oligomerization of three-bridged complexes based on the results of mass spectrometry. Through the analysis of non-valent interactions in the structures,  $\pi$ -stacking, halogen- $\pi$  and CH- $\pi$  interactions were found. An analysis of the Hirshfeld surface for  $[\{\text{TcOCl}_2\}_2(\mu\text{-O})(\mu\text{-pyd})_2]$ ,  $[\{\text{TcOCl}_2\}_2(\mu\text{-O})(\mu\text{-trz})_2]$  and their rhenium analogues showed that the main contribution to the crystalline packing is made by interactions of the type  $\text{Hal}\cdots\text{H}/\text{H}\cdots\text{Hal}$  (45.4–48.9%),  $\text{H}\cdots\text{H}$  (10.2–15.8%), and  $\text{O}\cdots\text{H}/\text{H}\cdots\text{O}$  (9.4–16.5%).



**Citation:** Novikov, A.P.; Volkov, M.A. New O- and N-N-Bridging Complexes of Tc(V), the Role of the Nitrogen Atom Position in Aromatic Rings: Reaction Mechanism, Spectroscopy, DTA, XRD and Hirshfeld Surface Analysis. *Int. J. Mol. Sci.* **2022**, *23*, 14034. <https://doi.org/10.3390/ijms232214034>

Academic Editors: Attila Bende and Mihai V. Putz

Received: 17 October 2022

Accepted: 10 November 2022

Published: 14 November 2022

**Publisher's Note:** MDPI stays neutral with regard to jurisdictional claims in published maps and institutional affiliations.



**Copyright:** © 2022 by the authors. Licensee MDPI, Basel, Switzerland. This article is an open access article distributed under the terms and conditions of the Creative Commons Attribution (CC BY) license (<https://creativecommons.org/licenses/by/4.0/>).

**Keywords:** technetium; pyridazine; triazole; dimethylpyrazole; pyrimidine; technetyl; XRD-analysis; Hirshfeld surface analysis;  $\pi$ -interactions; metal-nitrogen bond; supramolecular chemistry

## 1. Introduction

Technetium is chemically and environmentally available as  $\text{TcO}_4^-$  and exhibits pronounced oxidizing properties in reactions. Depending on the reducing conditions  $\text{Tc(VII)O}_4^-$  may convert to stable/unstable final/intermediate species of Tc(V), Tc(VI) or Tc(III). In special cases, the products could be either of a cluster nature [1], or carbonyl derivatives [2,3] of Tc [2+, 2.5+ and 0] oxidation states. The close attention of researchers is attracted by Tc(V) and Tc(III) complexes; they play the most important roles in the preparative [4–6], radiopharmaceutical [7,8] and industrial reprocessing chemistry of Tc [9].

Great interest in technetyl (V) arose in connection with its use in nuclear medicine as a biologically active  $^{99\text{m}}\text{Tc}$  radiopharmaceutical based on the formation of Tc(V) coordination compounds [10–15]. Tc complexes with amine and imine ligands are the main models of Tc binding to amino acids, proteins, antibodies, etc. Tc(V) usually forms  $\text{trans-}[\text{O}_2\text{L}_4\text{Tc}]^+$  [10,16,17],  $[\text{OL}_n\text{Tc}]^+$  [18,19], and  $[\text{TcNL}_n]$  [20,21] where L is an N-containing organic ligand.

Many organic compounds based on heterocyclic molecules have bactericidal and cytotoxic characteristics, and they are frequently found in biological systems. Halogen atoms are frequently found in organometallic complexes, and the structure of the complexes might vary depending on the type of heterocyclic ligand used. There were no references to Tc(V) compounds with the same structure as the previously reported Re(V) compounds, in which the rhenium atoms were linked by three bridges, two of which formed a heterocyclic ligand [22–26]. The formation of Re(V) alkoxy compounds with heterocyclic ligands is also mentioned in the literature, though only a few examples have been described for technetium [27]. The association of these two types of compounds is discussed in works describing alkoxy-Re(V) compounds, as well as works describing the formation of Re(V) complexes with bridging ligands. Several groups have observed some general patterns in the formation of such molecules. The authors of Reference [28] propose that the production of Re-O-Re dimeric complexes occurs in the presence of water and that interaction with alcohols can result in alkoxy derivatives. Based on reactions involving Re(V) molecules, O=Re=O compounds are thought to constitute the final byproducts. Similarly, the authors of References [29,30] mention the production of dimeric and alkoxy derivatives of Re (V).

Understanding the patterns of interaction of technetyl (V) with heterocyclic bases of various structures can be used to predict the behavior of radiopharmaceuticals in living organisms, calculate quantum chemical interactions of technetium compounds, and plan further chemical studies. Weak intermolecular interactions are of particular interest from a theoretical point of view, the study of such interactions in pertechnetates and perrhenates of purines led to the discovery of a new type of chemical bond [31,32]. New methods of separating perrhenates and pertechnetates are based on non-valent interactions [33–37]. The study of the non-valent interactions contribution for various technetium compounds will allow for a deeper understanding of the impact of radiopharmaceuticals on living organisms [7] and the formation of non-trivial technetium complex compounds, similar to those described in References [4,5,16,38]. Information about weak interactions can also be useful for predicting the behavior of Tc-containing intermediates in catalytic and sorption processes on complex organic sorbents like those described in Reference [39].

This work is devoted to the synthesis and characterization of a new, previously known for rhenium, type of technetium compound. Four new coordination compounds were obtained in the work: **1**—[ $\{\text{TcOCl}_2\}_2(\mu\text{-O})(\mu\text{-pyd})_2$ ], **2**—[ $\{\text{TcOCl}_2\}_2(\mu\text{-O})(\mu\text{-trz})_2$ ].Htrz·Cl, **3**—[ $\{\text{TcO}(\text{dmpz})_4\}(\mu\text{-O})(\text{TcOCl}_4)$ ], **4**—[ $\text{TcO}(\text{pyr})_2\text{Cl}_2(\text{OMe})$ ], where pyridazine (pyd), 1,2,4-triazole (trz), 3,5-dimethylpyrazole (dmpz) and pyrimidine (pyr). For the compounds obtained, some data on thermal stability, electron absorption spectroscopy of solutions, and infrared spectroscopy of the obtained powders are presented, as well as intermolecular interactions in crystals are considered by the Hirshfeld surface analysis. MALDY-ToF spectroscopy was performed on dried precipitates of mother liquor. All these methods, in combination with other experimental data presented in the paper, made it possible to develop a mechanism for the synthesis of Tc(V) organometallic complexes.

## 2. Results and Discussion

### 2.1. Structural Description of Tc(V) Complexes

The crystals of the compounds **1**, **3**, and **4** described below were mostly small-sized and poorly diffracted, and it seemed impossible to record the experiment with better quality even at low temperatures (100 K).

In all these compounds, the technetium atom exhibits an oxidation state of +5. In **1**, **2**, and **3**, the technetium atoms are linked to each other through an oxygen bridge. Moreover, in **1** and **2**, they are additionally linked by a Tc-N-N-Tc bond through the nitrogen atoms of the aromatic rings (Figure 1). In structure **2**, although the studied molecule of the complex is electrically neutral, the structure contains a triazolium cation and a chloride anion. All studied molecules of the complexes are electrically neutral. The Tc-N distances are close in **1** and **2** (in **1**, the Tc-N distances change from 2.15(2) to 2.19(2) Å, in **2** from 2.138(3) to 2.162(3) Å). The shortest Tc-N distance is observed in the complex with dimethyl

pyrazole (2.11(2) Å). The N-Tc-N angles in **1** are 90°, and in **2** they are slightly different from 90° (86° and 87°). At **3** and **4**, the N1-Tc1-N1<sup>1</sup> and N1-Tc1-N7 angles are 174° and 178°, respectively. In structures **1** and **2**, the Tc-O-Tc angles are equal to 128°, and in **3** this angle is 180°. The lengths of Tc-O bonds with bridging oxygen atoms are extended within one complex by 0.02–0.05 Å, the longest Tc-O bond is observed in **3** (1.95(7) Å), which may be related to another Tc2 environment. The lengths of Tc-O bonds with terminal oxygen atoms in **1**, **2**, and **4** are close (1.650(8)–1.67(2) Å). The largest elongation (1.69(4) Å) and shortening (1.62(4) Å) of the Tc-O bond is observed in **3**. The lengths of the Tc-Cl bonds in **1** and **2** are close, in **3** this bond is slightly longer (from 2.332(9)–2.345(1) Å to 2.397(5) Å). It should be noted that, in **4**, the length of the Tc1-Cl1 bond is close to **1**–**3** (3.371(3) Å), and the Tc1-Cl2 bond is slightly lengthened (2.450(3) Å).

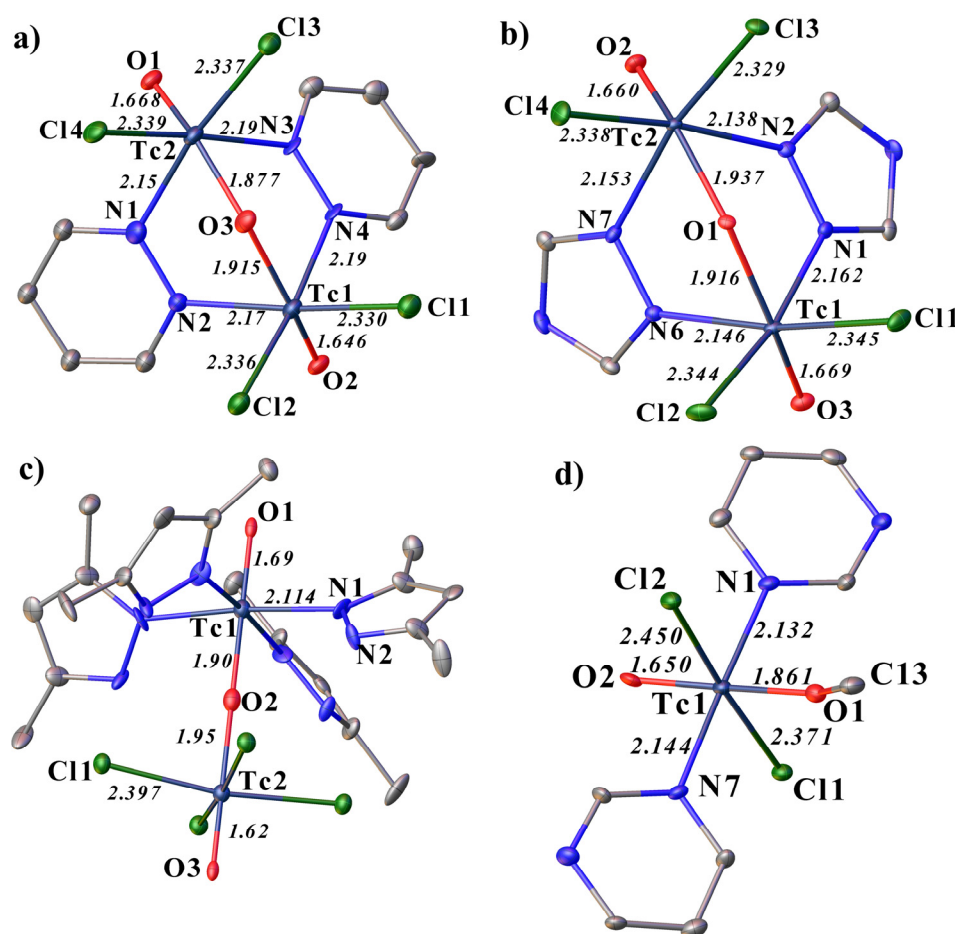


**Figure 1.** Molecular structure of **1** (a), **2** (b), **3** (c) and **4** (d) representing the coordination of the technetium atom with some bond lengths and labeling. Solvent molecules, counterions and H-atoms are omitted for clarity.

The N-N bond length in **1**–**3** varies from 1.33(3) to 1.40(3) Å; in **4** the N...N distance is 2.38(2) Å. An increase in the distance between the nitrogen atoms and a change in the angle between them can explain the formation of a different type of complex, which is different from **1** and **2**. In **3**, a different type of complex is formed, apparently due to the presence of a proton at one of the nitrogen atoms, as in a similar rhenium analogue [40].

The angles and distances in **1** are close to those described previously for the rhenium analog with pyridazine [24,25]. At the same time, for tetrazole, **2** compounds were not similar, as has been described in the literature, neither with a rhenium atom, nor with a technetium atom. Additionally, the compounds with dimethylpyrazole described for rhenium have a different geometry and structure [22,23,41–43].

In **1**, only weak hydrogen bonds of the C-H...Cl type are present between the molecules of the complex. In **2**, due to the presence in the structure, in addition to the molecule of the complex, charged cation and anion molecules, a more complex system of hydrogen bonds is formed than in **1**. The molecules of the complex are interconnected through chloride anions by H-bonds of the N-H...Cl type and are connected to triazolium cations by hydrogen bonds of the type C-H...Cl (Figure 2). In **3**, unlike **1** and **2**, intramolecular H-bonds of the N-H...Cl and C-H...N type are formed. In **4**, intermolecular hydrogen bonds of the C-H...O type are formed. In **4**, the molecules of the complex are additionally interconnected by a  $\pi$ -stacking interaction between C2N1C6C5C4N3 and C8N7C12C11C10N9<sup>1</sup> (symmetry code:  $x, 1 + y, z$ ) rings (angle: 5.6(4)°, centroid-centroid distance: 3.586(7) Å, shift distance 0.84(1) Å), which is absent in **1–3** [16,44,45] (Figure 3a). However, in **3**, the methyl hydrogen of dimethylpyrazole participate in intramolecular CH- $\pi$  interaction (the distances between the hydrogen atoms and the centers of the aromatic rings are shorter than 3 Å (2.83(1) Å)) [16,46–49]. Additionally, in **1** there are halogen- $\pi$  interaction with Cl...ring-center distance 3.90(1) Å and Cl...C distance 3.35(3) Å (which is shorter than the sum of van der Waals radii equal to 3.45 Å) [50–55]. Crystal packing in all compounds can be represented as layered.

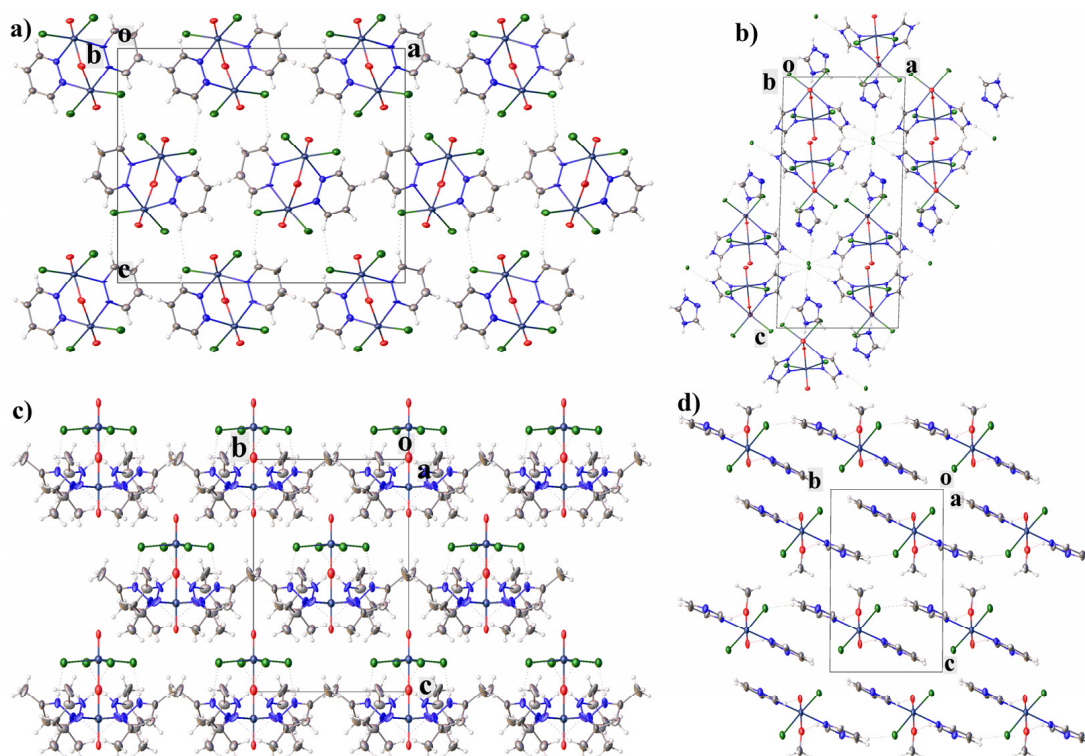


**Figure 2.** Crystal packing of **1** (a), **2** (b), **3** (c) and **4** (d) showing the complexes' layers.

## 2.2. Hirshfeld Surface Analysis

Hirshfeld surface (HS) analysis is based on the division of the electron density in a crystal. The Hirshfeld surface covers the molecule and determines the volume of space in which the electron density of the promolecule exceeds the density of all neighboring molecules [56]. This method can be used to analyze different types of non-valent interactions [32,57–61].

The Crystal Explorer 21 [62] program was used to analyze non-valent interactions in crystals using the HS analysis. The donor-acceptor groups are visualized using a standard (high) surface resolution and  $d_{\text{norm}}$  surfaces (Figure 4a–d). Red spots on the  $d_{\text{norm}}$  surface correspond to contacts shorter than the sum of van der Waals radii, such as hydrogen bonds,  $\pi$ -stacking or CH- $\pi$  interactions and blue ones, respectively, are longer than the sum

of van der Waals radii. For the additional analysis of  $\pi$ -stacking interactions, shape-index surfaces were constructed for all the complexes. Only **4** has characteristic red and blue triangles on the shape-index surface corresponding to the  $\pi$ -stacking interaction, which are absent for **1–3** (Figure 4e,f).

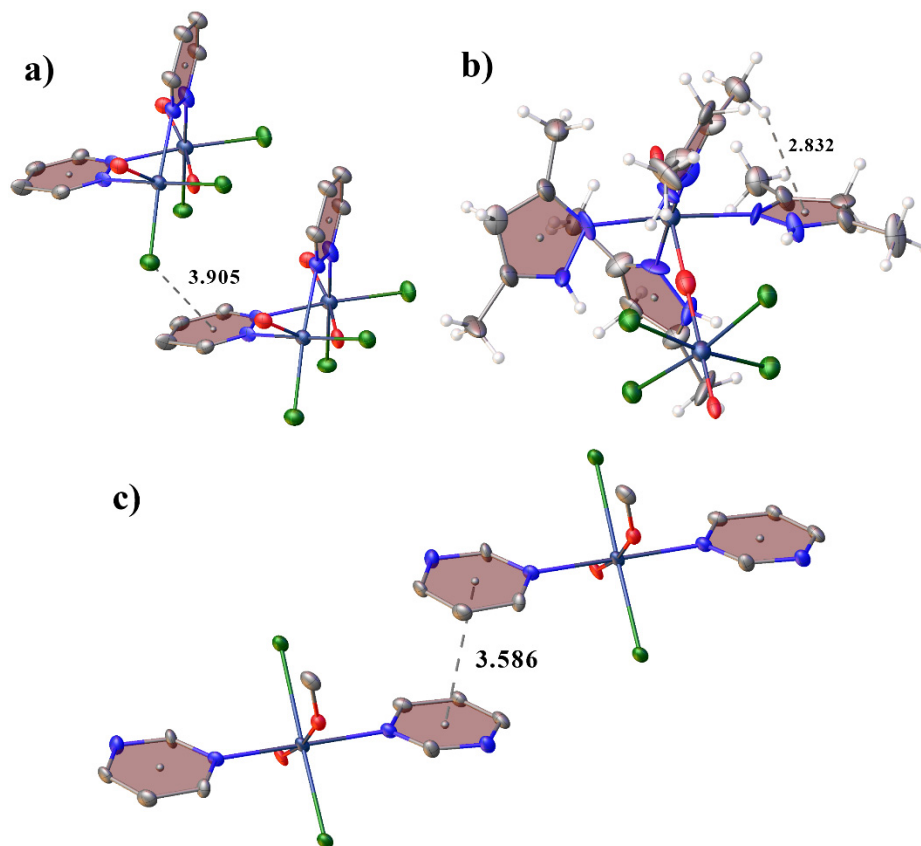


**Figure 3.** View showing halogen- $\pi$  in **1** (a), CH- $\pi$  in **2** (b) and  $\pi$ -stacking interactions in **3** (c). H-atoms are omitted for clarity in (a,b).

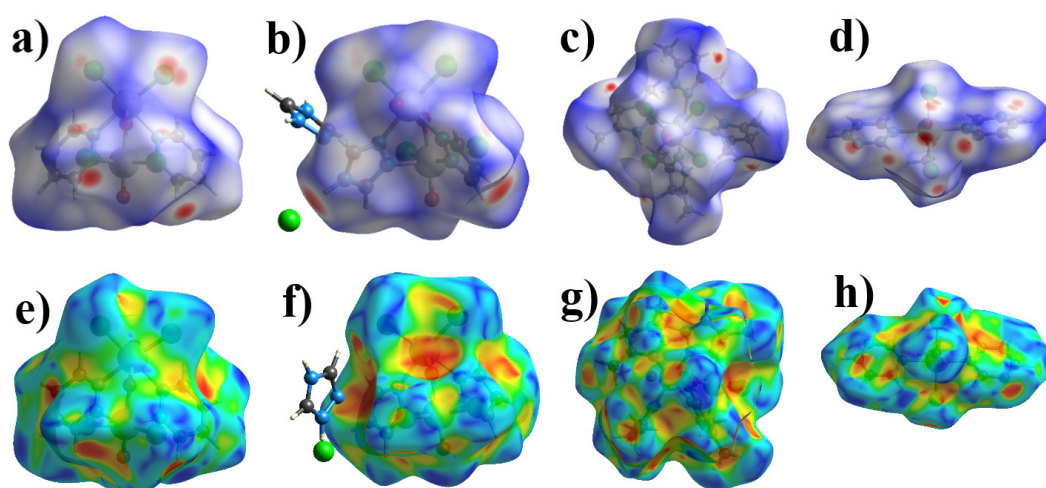


**Figure 4.** HS mapper over  $d_{\text{norm}}$  for **1** (a), **2** (b), **3** (c) and **4** (d) and HS mapper shape-index of **1** (e), **2** (f), **3** (g), and **4** (h) to visualize of intermolecular interactions in crystals.

We have analyzed the HS for analogues of the **1** and **2** compounds. Since no compounds like **1** and **2** are known for technetium (as well as for manganese), we decided to compare the contribution of non-valent interactions in **1–4** with rhenium analogs of

1–2 found in the Cambridge Structural Database [63]. With rhenium atoms, as mentioned above, only analogues with pyridazine, which connects rhenium atoms with an N–N bond, were found [24,25]. In all structures found, apart from complex molecules, solvent molecules such as acetone (HAWFUH: ( $\mu$ 2-oxo)-bis(dibromo-bis(pyridazine)-oxo-rhenium) acetone solvate [24]), benzyl (VIHWOZ: ( $\mu$ 2-Oxo)-bis( $\mu$ 2-pyridazine)-tetrachloro-dioxo-di-rhenium(v) benzene solvate [25]), or acetonitrile (VIHWUF: ( $\mu$ 2-Oxo)-bis( $\mu$ 2-pyridazine)-tetrabromo-dioxo-di-rhenium(v) acetonitrile solvate [25]) crystallized. However, at the same time, for 1–2 and for analogues, the main contribution to intermolecular interactions is made by contacts of the Hal $\cdots$ H/H $\cdots$ Hal type (Figure 5). The largest contribution of this type of interaction is observed for 2 (48.9%). In 3 and 4, the share of this type of interactions is almost the same (25.5 and 25.2%) and almost two times less than in 1 and 2. Van der Waals interactions of the H $\cdots$ H type make almost the same contribution to 1 (10.2%) and 2 (10.4%), but much more to the rhenium analogs. The greatest contribution to intermolecular interactions in 3 is made, in contrast to 1 and 2, by H $\cdots$ H interactions (65.8%). At the same time, the proportion of this type of interaction in 4 is also significant (30.0%) and more than in 1 and 2. For 1, in contrast to other complexes, contacts of the C $\cdots$ Hal/Hal $\cdots$ C type (which are usually responsible for  $\pi$ -halogen interactions) make a large contribution, which may be due to the absence of solvent molecules or other ions in the structure. The contacts of the O $\cdots$ H/H $\cdots$ O type play an important role in non-valent interactions in rhenium analogs (16.5% and 11.6%), and account for only 5% in 2 and 9.4% in 1. Contacts of the O $\cdots$ N/N $\cdots$ O type make a significant contribution to 4 (16.8%), in contrast to the other compounds. In 4, contacts of the C $\cdots$ C type appear, which are responsible for the pi-stacking interaction. The contacts of the O $\cdots$ Hal/Hal $\cdots$ O type make the same contribution to 1 and 2 (8.3%), in the HAWFUH only 4.8%, while the rest are practically absent. It is worth mentioning that Br $\cdots$ Br-type contacts appear in VIHWUF, which are absent in 1 and 2 (these contacts are usually responsible for halogen bonds). Contacts that contribute less than 2% are not considered in Figure 5.

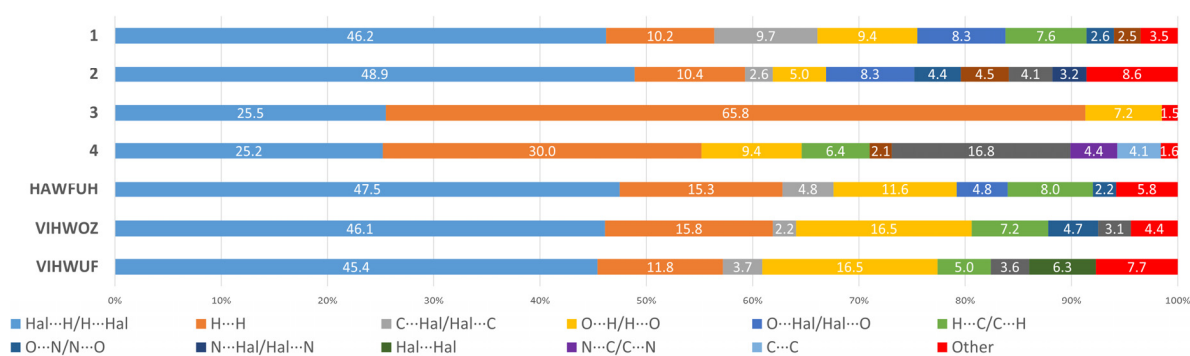


**Figure 5.** Percentage contributions of contacts to the Hirshfeld surface in structures 1–4 and analogues taken from CSD. HAWFUH: ( $\mu$ 2-oxo)-bis(dibromo-bis(pyridazine)-oxo-rhenium) acetone solvate [24]; VIHWOZ: ( $\mu$ 2-Oxo)-bis( $\mu$ 2-pyridazine)-tetrachloro-dioxo-di-rhenium(v) benzene solvate [25]; VIHWUF: ( $\mu$ 2-Oxo)-bis( $\mu$ 2-pyridazine)-tetrabromo-dioxo-di-rhenium(v) acetonitrile solvate [25].

### 2.3. Spectroscopic Studies

Electron absorption spectroscopy of a methyl solution of  $\text{NH}_4\text{TcO}_4$  in concentrated hydrochloric acid (Figure 6, curve 1) showed the presence of bands at 482, 414, 396, and 296 nm, indicative of Tc compounds in the reduced Tc(V) form, with an error of  $\pm 7$  nm. An additional band at  $245 \pm 2$  nm is found in the spectrum, which is characteristic of Tc(VII). UV-Vis spectroscopy of acetone and tetrahydrofuran solutions containing Tc(V) compounds was performed to clarify the peculiarities of the behavior of technetium compounds in the context of the reaction of complex compound synthesis with the participation of alcohols. Unlike methanol, all spectral bands were implicit; in the visible spectrum region, intense absorption occurs in the range from 500 to 350 nm, which is typical for Tc(V). Figure 6 illustrates the curves taken in a methanol/acetone solution. The addition of

equimolar amounts of heterocyclic ligands to acetone solutions of technetium compounds (using 2,5-dimethylpyrazole and 1,2,4-triazole as examples) did not result in a band shift, indicating the absence of a complex formation reaction in the first minutes after the ligand was added.

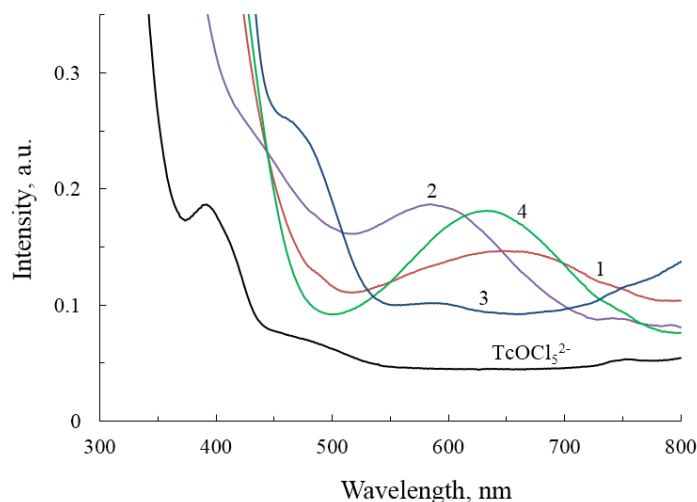


**Figure 6.** Electron absorption spectroscopy of mother methanol solutions of complexes: Compound 1—curve 1; compound 2—curve 2; compound 3—curve 3; compound 4—curve 4; and stock solution  $(\text{NH}_4)_2\text{TcOCl}_5$ . The concentration of technetium in the solutions was equal and amounted to approximately 0.01 M.

During the initial minutes of the reaction, broad absorption bands in the range of 587–650 nm were detected in the dilute stock solutions of compounds 1, 2, 3, and 4 by UV-Vis spectroscopy. Bands of the original compound Tc(V) (Figure 6) cannot be detected; the available bands corresponding to technetium halide complexes are displaced to the low-energy region and range from 400 to 500 nm. For complex 1, two bands at 491 and 652 nm are recorded (Figure 6, curve 1); for complex 2, two bands at 445 and 595 nm (curve 2); for complex 3, two bands at 470 and 600 nm (curve 3); for complex 4, one band was recorded with a peak at 635 nm (curve 4). The literature describes UV-Vis spectroscopy for compounds similar to complexes 1 and 2 obtained for Re(V). The spectra [22] likewise exhibits a broad band at 645 nm. The authors of [22] attribute the band around 645 nm to the significant character of the ligand field ( $5d_{xy} \rightarrow d_{xz}, d_{yz}$ ) [64,65]. Spectroscopy of compound 3 displays a wave similar to  $\text{TcO}_2\text{Cl}_4$  halide complexes, as well as a band in the longer wavelength region similar to  $\text{TcO}_2\text{L}_4$  compounds, where L is an N-containing ligand; a comparable spectrum was recorded for  $\text{TcO}_2(\text{Im})_4^+$  compounds [16].

Based on the data presented, it can be concluded that technetium compounds  $\text{X}_n\text{Tc}^{\text{V}}_2(\mu\text{-O})(\mu\text{-N-N})_2$  have absorption in the 600–650 nm range. However, if the molecule is not doubled by bridging ligands, the absorption wave shifts to a shorter wavelength region. It is impossible to interpret the results, since the heterocyclic compounds used in the work absorb intensely in the near UV range. The design of curves 1 and 2 suggests that distinct structural products from those isolated in the form of crystals may develop.

The extinction coefficients for compounds 1, 2, 4 were calculated from absorption bands in the range  $600 \pm 50$  nm. For compound 3, were calculated from the absorption band at 470 nm. Technetium concentrations were equal in all cases ( $c = 0.01$  M), only one cell ( $l = 10.001$  mm) participated in the experiment. The calculated extinction coefficients for compounds 1, 2, 3, and 4 ( $\text{M}^{-1} \text{cm}^{-1}$ ) were: 3.47, 9.89, 15.63, and 10.38, respectively.

Infrared spectroscopy of the obtained complexes showed the presence of multiple bands corresponding to organic heterocycles. The IR spectra of the complexes are shown in Supplementary Materials Figure S2. The intense absorption near  $1100 \text{ cm}^{-1}$ , a feature of stretching vibrations of the C-N bond and stretching vibrations of C-H bonds in the range of  $2800$  to  $3050 \text{ cm}^{-1}$  are also present in the spectra of all compounds. The C-C bond of

aromatic heterocycles exhibits strong absorption bands in the range of 1570–1625  $\text{cm}^{-1}$  in the spectra of compounds **1**, **3**, and **4**. Stretching vibrations of the N-N bond may be responsible for the low-intensity absorption bands in the complexes **1** and **2** spectra between 1400 and 1500  $\text{cm}^{-1}$ . Compounds **3** and **4**'s spectra exhibit absorption bands at 1430 and 1470  $\text{cm}^{-1}$ , respectively, which indicate the  $\text{CH}_3$  group's bending vibrations. Compound **4** has an absorption line of stretching vibrations of the C-O bond at 1020  $\text{cm}^{-1}$  in its spectra. N-H vibrations are indicated by a broad peak in the 3300–3450  $\text{cm}^{-1}$  region, which is only observed in the spectra of compound **2**. Additionally, all spectra can exhibit the long-wavelength waves of lingering water. Table S16 in the Supplementary Materials contains a complete list of peaks.

The Tc-N and Tc-Cl bond vibrations could not be detected on the spectra since the region specific to these vibrations (200–500  $\text{cm}^{-1}$ ) was uninformative. All of the reported compounds' spectra have distinct bands for Tc=O vibrations in the 790–950  $\text{cm}^{-1}$  region [18,66].

#### 2.4. MALDI-ToF Analysis of the Mother Liquor of **1**

Mass spectrometry was performed on the dried residues of component 1 stock solutions. The mass spectrum contains peaks with a maximum mass of 970 a.m.u., which, based on isotope distribution, correspond to the pyridazine resinification side processes and are not depicted in Figure 7. Peaks corresponding to chlorine and oxo derivatives of organic pyridazine fragments generated during laser desorption of the material under study are recorded with a high degree of probability in the mass range up to 251 a.m.u., with the exception of peaks in the region of 247 a.m.u. Peaks with proposed suitable formulas and structures are labelled as black in Figure 8 and are reported in the Supplementary Materials (Table S17). Red-labelled peaks were not interpreted and were excluded from the table.

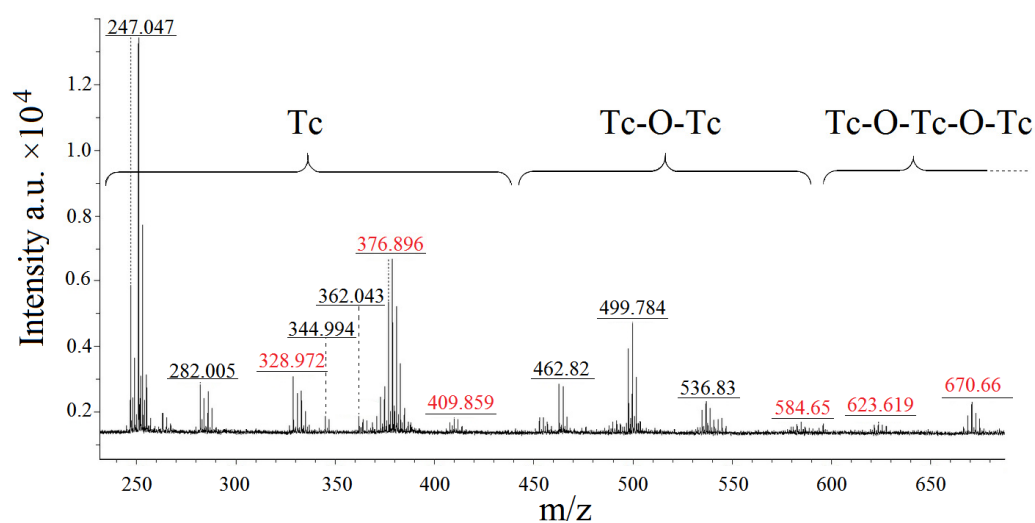


**Figure 7.** MALDI spectroscopy of the stock solution of compound **1**.

According to the quantity of technetium atoms, the peaks in the spectrum were split into three groups. Complexes with only one technetium atom in their structure belong to the first category, which spans the 247–440 a.m.u. range. Peaks 247.047 a.m.u. (calc. 246.05) and 282.005 a.m.u. (calc. 281.98) correspond to particles with the gross formulas  $\text{TcO}_2\text{ClN}_2\text{C}_4\text{H}_5$  and  $\text{TcO}_2\text{Cl}_2\text{N}_2\text{C}_4\text{H}_5$ , respectively. Since each of these particles contains one heterocyclic fragment, it is possible that the formation of particles with only one heterocyclic fragment in their structure is one of the initial steps in the reaction for compound **1**. The gross formulas for the peaks at 344.94 a.m.u. (calc. 344.97) and 362.043 a.m.u. (calc. 361.99) are  $\text{TcOCl}_2\text{N}_4\text{C}_8\text{H}_8$  and  $\text{TcO}_2\text{Cl}_2\text{N}_4\text{C}_8\text{H}_9$ , respectively. The particles include two heterocycles, and the structures differ by one OH fragment.

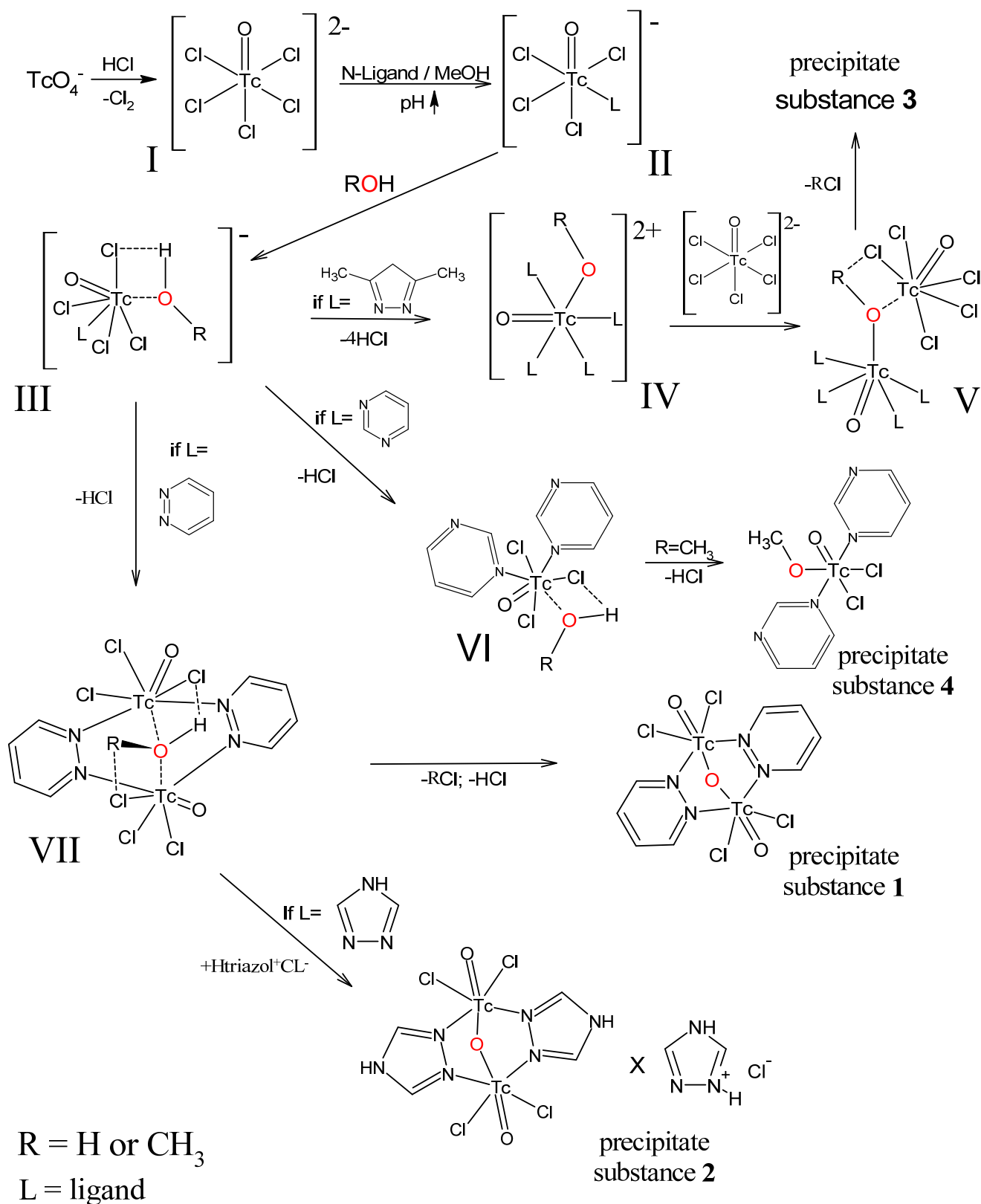


**Figure 8.** Proposed mechanism for the formation of compounds 1, 2, 3 and 4.

The second group has a mass range of 450–590 a.m.u., and the associated particles have two technetium atoms joined by ligand and/or oxygen bridges. The fragments with peaks 462.82 (calc. 462.75), 499.784 (calc. 499.777), and 536.83 (calc. 536.79) likely preserve

the Tc=O fragment and include one heterocycle each. With this assumption, we may assign the gross formulas  $\text{Tc}_2\text{O}_5\text{Cl}_3\text{N}_2\text{C}_4\text{H}_4$ ,  $\text{Tc}_2\text{O}_5\text{Cl}_4\text{N}_2\text{C}_4\text{H}_4$  and  $\text{Tc}_2\text{O}_5\text{Cl}_5\text{N}_2\text{C}_4\text{H}_6$ .

The third cluster of peaks is between 600 and 700 a.m.u. in mass, and the particles in this cluster include three technetium atoms connected by distinct types of bridges. The interpretation of heavy peaks is problematic; nevertheless, based on the nature of the isotopic distribution, fragments with a mass more than 600 a.m.u. can be presumed to have three technetium atoms in their structure. Three-bridge complexes Tc(V) can apparently oligomerize through ligand bridges.

### 2.5. Proposed Mechanism for the Formation of Complexes

The major anion generated during the  $\text{TcO}_4^-$  reduction reaction in concentrated hydrochloric acid is the  $\text{TcOCl}_5^{2-}$  specie I, which is typical of the transition metals in the +5-oxidation state (Figure 8). The addition of a heterocyclic base solution changes the pH of the medium and initiates hydrolytic activities with the creation of specie II. A methanol or water molecule is oriented towards specie II through a chlorine atom via a  $\text{Cl}\cdots\text{H}$  hydrogen bond, while the ligand's distortion of specie II can create conditions for nonvalent interactions of the oxygen atom with the metal atom and the formation of specie III. It should be noted that an excess of water can cause complete hydrolysis of technetium-containing specie and the formation of colloidal suspensions. The structure of the ligand influences the subsequent reaction with a heterocyclic base. Interaction with 2,5-dimethylpyrazole results in the substitution of three chlorine atoms and the production of Tc-N bonds, as well as the elimination of hydrochloric acid and the formation of the Tc-O link. Hydrolytic activities involving 2,5-dimethylpyrazole that result in the synthesis of specie IV appear to proceed swiftly; this can explain the presence of Tc(V) compounds in solution in diverse chemical forms, resulting in the formation of specie V. The formation of an oxygen bridge apparently occurs with the elimination of MeCl or HCl, this stage of the process is the rate-limiting one. Experiments have shown that the interaction of technetyl halide complexes with five-membered heterocycles can give several products of various structures, which are not discussed in this paper.

In the case of six-membered heterocycles, if the heteroatoms in the cycle are not conjugated, the formation of ligand bridges does not occur. Compound 4 is insoluble in alcohols. Hydrolytic reactions stop when only two chlorine atoms are replaced by pyrimidine. Since there is no delayed methyl chloride production stage, precipitation occurs relatively quickly. It is reasonable to expect that using a six-membered pyrazine heterocycle as a ligand will result in the creation of a compound similar to 4. In the presence of conjugated heteroatoms in the cycle, such as pyridazine, Tc-N-N-Tc bridges and specie VII form. In the case of the formation of a complex, paired molecule, the formation of bridging oxygen and the elimination of HCl or MeCl become possible, which leads to a fairly rapid precipitation.

For 1,2,4-triazole, the process is seen in various ways. However, due to compound 2's low solubility, the equilibrium shifts towards the reaction product. However, the crystallization process takes longer than expected, and is likely caused by extra non-valent interactions of the nitrogen atom in position 4, and as a result, the substance crystallizes alongside 1,2,4-triazole hydrochloride.

The formation of the described compounds leads to the conclusion that the mechanism of  $\text{TcO}_2(\text{Im})_4^+$  imidazole compound formation proposed in Reference [16] can only be correct at the stages of reduction of Tc(VII) with thiourea. Based on the suggested mechanism for compound 3, it can be assumed that the solvent also plays a role in the formation of  $\text{TcO}_2(\text{Im})_4^+$  compounds.

### 2.6. DTA-Analysis

The active phases of complexes 1, 2, and 3 decomposition occur in the range of 250–525 °C, according to TG-DTA analysis data. According to pXRD data, the thermolysis of all the compounds described in the study in an argon-hydrogen mixture atmosphere

resulted in metallic technetium and an unidentified phase that contains technetium, oxygen, chlorine, and carbon atoms, according to X-ray fluorescence spectroscopy data. The decomposition temperatures of compounds **1**, **2** and **3** are 283 °C, 225 °C and 185 °C, respectively (Figure 9). Compounds **1**, **2**, and **3** lost 35%, 51%, and 55% of their total weight. Unfortunately, despite the relatively substantial weights of complexes **1–3** samples collected for thermal analysis (5 mg each); the data obtained were uninformative. Thermal analysis data for compounds **1** and **2** are provided in Figures S3 and S4 in the Supplementary Materials.

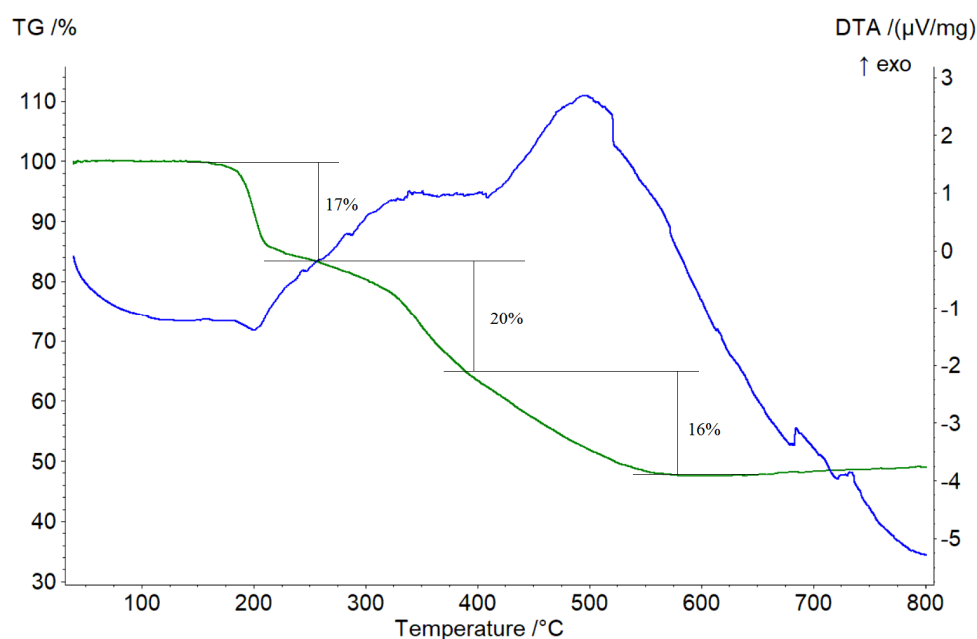


**Figure 9.** TG–DTA decomposition data of  $\text{TcO}(\text{Pyr})_2\text{Cl}_2\text{OMe}$  in the  $\text{Ar-H}_2$  atmosphere.

The active phase of compound **4** decomposition occurs in the temperature range of 180–530 °C, according to TG-DTA analysis data. The extrapolated temperature of the decomposition starts at 180 °C. Depending on the shape of the TG curve, at least three partially overlapping stages of the decomposition process can be distinguished. A weight loss of around 17% is seen in the 180–215 °C temperature range, and the decomposition process proceeds with heat absorption with a maximum in 200 °C. Further heating results in a slow decrease in mass to a temperature of 317 °C, which could be attributed to residual effects from the initial stage of decomposition, but no energy effects appear on the DTA curve. The second stage of decomposition occurs in the range of 320–380 °C, the weight loss is approximately 20%, while an unexpressed exothermic effect is observed on the DTA curve. The third phase of decomposition proceeds in the temperature range of 380–530 °C and is accompanied by heat emission. Further heating resulted in sample mass stabilization. During heating, the total weight loss was 53%. According to pXRD analysis, the residue was primarily composed of metallic technetium.

### 3. Materials and Methods

*Caution!*  $^{99}\text{Tc}$  is a  $\beta$ -emitter ( $A = 635 \text{ Bq}/\mu\text{g}$  [67],  $E_{\text{max}} = 290 \text{ keV}$ ); appropriate shielding and manipulation technics were employed during the synthesis and in all manipulations.

Pyrimidine, 2,5-dimethylpyrazole, pyridazine, triazole were purchased from Sigma-Aldrich (Darmstadt, Germany). All reagents and solvents were qualified chemically pure and were not subjected to further purification.

The ammonium pertechnetate (ISOTOP RF) used in the work was recrystallized from bidistilled water ( $R \geq 18 \text{ M}\Omega$ ). The resulting white crystalline powder was especially pure and spectrally pure.

### 3.1. Synthesis of Complexes

Finely milled dry  $\text{NH}_4\text{TcO}_4$  was dissolved in a minimum amount of concentrated hydrochloric acid (12 M). The resulting solution was evaporated to half at room temperature in the vacuum of an oil pump, while chlorine was intensively released from the solution. The residual greenish-yellow solution was diluted with methanol in a ratio of 2:1, and the appropriate heterocyclic ligand methanol solutions were slowly added to the resulting mixture under vigorous stirring until a saturated green color was formed. During the synthesis of compounds **1** and **4**, a precipitate began to form 2–3 min after the addition of the first drops of the ligand solution. For compound **2**, the formation of a precipitate began 12 h after the start of the reaction. Compound **4** was formed only upon evaporation of the mother liquor to half its volume. The resulting compounds were washed with methanol and air dried. The reaction yields were calculated relative to Tc as follows: **1**, **4**—95%, **2**—75%, and **3**—62%.

The elemental analysis calculated/found (%): For **1** Tc—36.11/37.73, C—17.54/17.81, N—10.23/10.05; for **2** Tc—31.24/32.65, C—11.38/11.43, N—19.91/19.85; for **3** Tc—25.55/26.67, C—31.03/31.1, N—14.47/14.2; for **4** Tc—26.23/27.26, C—28.67/28.9, and N—14.86/14.74.

The initial technetium and ligand solutions were diluted 20 times with methanol to create crystals **1** and **4** acceptable for sXRD analysis. After mixing, a barely perceptible green tint developed, and the crystals started to form 50–70 min later.

### 3.2. Single-Crystal XRD Analysis

The crystal structure of all synthesized substances was determined by X-ray structural analysis using an automatic four-circle area-detector diffractometer Bruker KAPPA APEX II with  $\text{MoK}\alpha$  radiation. The cell parameters were refined over the entire data set, together with data reduction using SAINT-Plus software [68]. Absorption corrections were introduced using the SADABS program [69]. The structures were solved using the SHELXT-2018/2 program [70] and refined by full-matrix least squares on  $F^2$  in the anisotropic approximation for all non-hydrogen atoms (SHELXL-2018/3 [71]). Atoms H, bounded to CH- and NH- groups, were placed in geometrically calculated positions with isotropic temperature factors equal to  $1.2 U_{eq}(\text{C}, \text{N})$  and  $1.5 U_{eq}(\text{C})$  for  $\text{CH}_3$ -groups. The H atoms in NH- groups in **2** were objectively located from the difference Fourier synthesis and refined with isotropic temperature factors equal  $1.2 U_{eq}(\text{N})$ . Structure **1** was refined as an inversion twin. Tables and figures for the structures were generated using Olex2 [72].

Crystal data, data collection, and structure refinement details are summarized in Table 1. All other crystallographic parameters of the structures are indicated in Tables S1–S15. The atomic coordinates were deposited at the Cambridge Crystallographic Data Centre [63], CCDC No. 2213501–2213504 for **1–4**. The Supplementary crystallographic data can be obtained free of charge from the Cambridge Crystallographic Data Centre via [www.ccdc.cam.ac.uk/data\\_request/cif](http://www.ccdc.cam.ac.uk/data_request/cif) (accessed on 10 October 2022).

**Table 1.** Crystal data and structure refinement for structures **1–4**.

Identification Code	1	2	3	4
Empirical formula	$\text{C}_8\text{H}_8\text{Cl}_4\text{N}_4\text{O}_3\text{Tc}_2$	$\text{C}_6\text{H}_{10}\text{Cl}_5\text{N}_9\text{O}_3\text{Tc}_2$	$\text{C}_{20}\text{H}_{36}\text{Cl}_4\text{N}_8\text{O}_3\text{Tc}_2$	$\text{C}_9\text{H}_{11}\text{Cl}_2\text{N}_4\text{O}_2\text{Tc}$
Formula weight	545.98	631.30	774.37	376.12
Temperature/K	100(2)			
Crystal system	orthorhombic	monoclinic	tetragonal	triclinic
Space group	$Pna2_1$	$P2_1/n$	$I4$	$P-1$
a/Å	17.929(2)	10.4766(9)	10.059(6)	6.168(3)
b/Å	6.1567(9)	8.4060(7)	10.059(6)	8.617(4)

Table 1. Cont.

Identification Code	1	2	3	4
$c/\text{\AA}$	14.726(2)	21.6695(18)	15.055(13)	13.054(6)
$\alpha/^\circ$	90	90	90	89.553(17)
$\beta/^\circ$	90	91.572(3)	90	89.505(19)
$\gamma/^\circ$	90	90	90	69.338(16)
Volume/ $\text{\AA}^3$	1625.5(4)	1907.6(3)	1523(2)	649.2(5)
Z	4	4	2	2
$\rho_{\text{calc}}/\text{cm}^3$	2.231	2.198	1.688	1.924
$\mu/\text{mm}^{-1}$	2.368	2.176	1.294	1.519
F(000)	1048.0	1216.0	780.0	372.0
Crystal size/ $\text{mm}^3$	$0.3 \times 0.12 \times 0.05$	$0.22 \times 0.09 \times 0.06$	$0.06 \times 0.05 \times 0.04$	$0.39 \times 0.12 \times 0.04$
Radiation	MoK $\alpha$ ( $\lambda = 0.71073$ )			
2 $\theta$ range for data collection/ $^\circ$	8.494 to 54.986	8.326 to 59.998	9.078 to 59.994	9.37 to 59.982
Index ranges	$-23 \leq h \leq 23, -7 \leq k \leq 7, -19 \leq l \leq 18$	$-14 \leq h \leq 14, -11 \leq k \leq 9, -30 \leq l \leq 30$	$-14 \leq h \leq 13, -13 \leq k \leq 13, -21 \leq l \leq 20$	$-7 \leq h \leq 8, -12 \leq k \leq 11, -18 \leq l \leq 18$
Reflections collected	18191	32465	3234	10884
Independent reflections	3664 [ $R_{\text{int}} = 0.1657, R_{\text{sigma}} = 0.1277$ ]	5544 [ $R_{\text{int}} = 0.0925, R_{\text{sigma}} = 0.0779$ ]	1764 [ $R_{\text{int}} = 0.1930, R_{\text{sigma}} = 0.3190$ ]	3691 [ $R_{\text{int}} = 0.1534, R_{\text{sigma}} = 0.2125$ ]
Data/restraints/parameters	3664/1/162	5544/0/239	1764/1/83	3691/0/165
Goodness-of-fit on $F^2$	1.025	1.023	0.941	0.986
Final R indexes [ $I > 2\sigma(I)$ ]	$R_1 = 0.0691, wR_2 = 0.1416$	$R_1 = 0.0426, wR_2 = 0.0734$	$R_1 = 0.0971, wR_2 = 0.1829$	$R_1 = 0.1046, wR_2 = 0.2348$
Final R indexes [all data]	$R_1 = 0.1262, wR_2 = 0.1680$	$R_1 = 0.0659, wR_2 = 0.0805$	$R_1 = 0.2371, wR_2 = 0.2429$	$R_1 = 0.1907, wR_2 = 0.2894$
Largest diff. peak/hole/ $e \text{\AA}^{-3}$	2.42/−1.45	0.97/−0.88	1.39/−1.28	3.04/−2.23
Flack parameter	0.5(2)		0.06(19)	

### 3.3. Spectroscopic Analysis

The IR spectrum of the compounds was registered at Nicolet IR200 FT-IR from the 2 mg sample pressed as a finely grounded mixture with 100 mg KBr and pressed at 50 kg/cm<sup>2</sup>.

UV-visible spectroscopy was studied using the Cary 100 Scan in the range from 900 to 300 nm. A 10 mm quartz cuvette was used for measurements. The cuvette width was 10.001 mm.

### 3.4. MALDI-ToF—Analysis

For the study, we used a mass-spectrometer Ultraflex II (Bruker) in the reflective mode on positive ions without the use of a matrix with an accelerating voltage of 25 keV. Desorption was performed by an Nd:YAG laser beam ( $\lambda = 355$  nm). The interpretation of the obtained spectra and the identification of individual peaks were carried out using the FlexAnalysis-3.3 program.

### 3.5. Thermal Analysis

We performed thermal gravimetry with simultaneous differential thermal analysis (TG-DTA) using a Netzsch STA Jupiter 449 F3 thermoanalytical complex. Heating was carried out at a rate of 10 °C/min in the temperature range 40–1000 °C. Al<sub>2</sub>O<sub>3</sub> crucibles

and W-Re sample carrier were used; the atmosphere was the Ar-1.5% H<sub>2</sub> mixture with a purity of  $\omega(\text{Ar} + \text{H}_2) = 99.999\%$ .

### 3.6. Elemental Analysis

The chemical composition of the compounds was determined on a sample of 50 mg each. The technetium in the compounds was determined by liquid scintillation on a Tri-Carb 3180 TR/SL instrument (PerkinElmer, Rodgau, Germany), using a HiSafe 3 scintillator; the measurement error did not exceed 5%. C, N, O were determined using the EA 3000 EuroVector analyzer (EuroVector, Pavia PV, Italy), the measurement error was not more than 10%. The contents of chlorine and hydrogen in the compounds was not measured.

## 4. Conclusions

Four new complex compounds of Tc(V) with heterocyclic compounds of various structures were synthesized and characterized:  $[\{\text{TcOCl}_2\}_2(\mu\text{-O})(\mu\text{-pyd})_2]$ ,  $[\{\text{TcOCl}_2\}_2(\mu\text{-O})(\mu\text{-trz})_2] \cdot \text{Htrz} \cdot \text{Cl}$ ,  $[\{\text{TcO}(\text{dmpz})_4\}(\mu\text{-O})(\text{TcCl}_4\text{O})]$  and  $[\text{Tc}(\text{pyr})_2\text{Cl}_2\text{O}(\text{OMe})]$ . In the electronic absorption spectra of binuclear complexes Tc(V) showed that the presence of ligand bridges shifts absorption waves to longer wavelengths compared to mononuclear complexes. The absorption waves of Tc(V) coordination compounds with heterocyclic ligands are in the range of 550–650 nm. Based on the results of mass spectroscopy, it can be assumed that the interaction of Tc(V) halide complexes with heterocyclic compounds, having conjugated nitrogen atoms in their structure, can lead to the formation of oligomers Tc(V) complexes with the masses of complexes over 600 a.m.u. The decomposition temperatures for the obtained compounds **1**, **2**, **3** and **4** were established: 283 °C, 225 °C, 185 °C and 180 °C, respectively.

The interaction of Tc(V) compounds with heterocyclic N-containing ligands usually leads to the formation of  $[\text{O}=\text{Tc}=\text{O}]^+$  compounds; however, compounds of various structures can be formed depending on the position of the heteroatoms. Heterocycles having two or more conjugated nitrogen atoms in their structure lead to the formation of additional ligand bridges that prevent the formation of  $\text{O}=\text{Tc}=\text{O}$  compounds. Six-membered heterocycles having non-conjugated heteroatoms in their structure in an alcoholic solution lead to the formation of Tc(V) alkoxy compounds with two coordinated heterocyclic ligands. Apparently, the formation of Tc(V) complexes with heterocyclic ligands requires the presence of water or alcohols in the solution. The synthesis of substituted complexes proceeds faster with five-membered heterocycles, which leads to the formation of complexes with technetium atoms surrounded by ligands of various natures.

In the crystal structures obtained in this work, it was shown that the Tc-N distances vary from 2.11 to 2.19 Å and do not depend on the mode of coordination of the heterocycle to the Tc atom. The largest Tc-N distance is observed for the complex with pyd. The molecules of the complexes are bound together into crystal structures, as a rule, due to weak hydrogen bonds (C-H...Cl/O) and other non-valent interactions ( $\pi$ -stacking, halogen- $\pi$  and CH- $\pi$ ). However, if there are cations and anions in the structure, binding occurs due to stronger H-bonds (N-H...Cl) through cations and anions. In  $[\{\text{TcO}(\text{dmpz})_4\}(\mu\text{-O})(\text{TcOCl}_4)]$  intramolecular H-bonds of the N-H...Cl and C-H...N type are formed. The analysis of non-valent interactions by the Hirshfeld surface method for  $[\{\text{TcOCl}_2\}_2(\mu\text{-O})(\mu\text{-pyd})_2]$ ,  $[\{\text{TcOCl}_2\}_2(\mu\text{-O})(\mu\text{-trz})_2]$  and their comparison with rhenium analogs showed that, regardless of the halogen, metal atom, or the presence of other molecules in the structures, contacts the Hal...H/H...Hal (45.4–48.9%) type.

**Supplementary Materials:** The following supporting information can be downloaded at: <https://www.mdpi.com/article/10.3390/ijms232214034/s1>.

**Author Contributions:** Conceptualization, A.P.N. and M.A.V.; methodology, M.A.V.; software, A.P.N.; validation, A.P.N. and M.A.V.; formal analysis, A.P.N.; investigation, A.P.N. and M.A.V.; resources, A.P.N.; data curation, A.P.N. and M.A.V.; writing—original draft preparation, A.P.N.; writing—review and editing, M.A.V. and A.P.N.; visualization, M.A.V. and A.P.N.; supervision, A.P.N.; project administration, A.P.N.; funding acquisition, A.P.N. All authors have read and agreed to the published version of the manuscript.

**Funding:** The study was supported by the Ministry of Science and Higher Education of the Russian Federation (program no. 122011300061-3).

**Institutional Review Board Statement:** Not applicable.

**Informed Consent Statement:** Not applicable.

**Data Availability Statement:** The data presented in this study are available on request from the corresponding author.

**Acknowledgments:** X-ray diffraction experiments were performed at the Center for Shared Use of Physical Methods of Investigation at the Frumkin Institute of Physical Chemistry and Electrochemistry, RAS.

**Conflicts of Interest:** The authors declare no conflict of interest.

## References

1. Volkov, M.A.; Fedoseev, A.M.; Krivoborodov, E.G.; Toropygin, I.Y.; German, K.E.; Grigoriev, M.S.; Kuznetsov, V.V.; Budantseva, N.A.; Novikov, A.P.; Mezhuev, Y.O. A new method for the synthesis of polynuclear carboxylate complexes of technetium (II, III). *J. Organomet. Chem.* **2022**, *957*, 122146. [\[CrossRef\]](#)
2. Alberto, R. From oxo to carbonyl and arene complexes; A journey through technetium chemistry. *J. Organomet. Chem.* **2018**, *869*, 264–269. [\[CrossRef\]](#)
3. Sidorenko, G.V.; Miroslovov, A.E. Higher Technetium(I) Carbonyls and Possibility of Using Them in Nuclear Medicine: Problems and Prospects. *Radiochemistry* **2021**, *63*, 253–262. [\[CrossRef\]](#)
4. Zegke, M.; Grödler, D.; Roca Jungfer, M.; Haseloer, A.; Kreuter, M.; Neudörfl, J.M.; Sittel, T.; James, C.M.; Rothe, J.; Altmaier, M.; et al. Ammonium Pertechnetate in Mixtures of Trifluoromethanesulfonic Acid and Trifluoromethanesulfonic Anhydride. *Angew. Chem. Int. Ed.* **2022**, *61*, e202113777. [\[CrossRef\]](#) [\[PubMed\]](#)
5. German, K.E.; Fedoseev, A.M.; Grigoriev, M.S.; Kirakosyan, G.A.; Dumas, T.; Den Auwer, C.; Moisy, P.; Lawler, K.V.; Forster, P.M.; Poineau, F. A 70-Year-Old Mystery in Technetium Chemistry Explained by the New Technetium Polyoxometalate  $[H_7O_3]_4[Tc_{20}O_{68}] \cdot 4H_2O$ . *Chem. Eur. J.* **2021**, *27*, 13624–13631. [\[CrossRef\]](#) [\[PubMed\]](#)
6. Abram, U.; Beyer, R.; Münze, R.; Stach, J.; Kaden, L.; Lorenz, B.; Findeisen, M. Mixed-ligand complexes of technetium-III. Synthesis and characterization of [bis(diphenylphosphino)ethane]tetrakis(trimethylphosphite)technetium(I) hexafluorophosphate,  $[Tc(DPPE)(TMP)_4]PF_6$ . *Polyhedron* **1989**, *8*, 1201–1204. [\[CrossRef\]](#)
7. Duatti, A. Review on  $^{99m}Tc$  radiopharmaceuticals with emphasis on new advancements. *Nucl. Med. Biol.* **2021**, *92*, 202–216. [\[CrossRef\]](#)
8. Jürgens, S.; Herrmann, W.A.; Kühn, F.E. Rhenium and technetium based radiopharmaceuticals: Development and recent advances. *J. Organomet. Chem.* **2014**, *751*, 83–89. [\[CrossRef\]](#)
9. Melent'ev, A.B.; Mashkin, A.N.; German, K.E. The influence of deviations in process parameters on the purification of uranium from different radionuclides. *Theor. Found. Chem. Eng.* **2016**, *50*, 554–561. [\[CrossRef\]](#)
10. Fackler, P.H.; Lindsay, M.J.; Clarke, M.J.; Kastner, M.E. Synthesis and structure of trans- $[O_2(Im)_4Tc]Cl \cdot 2H_2O$ , trans- $[O_2(1-meIm)_4Tc]Cl \cdot 3H_2O$  and related compounds. *Inorg. Chim. Acta* **1985**, *109*, 39–49. [\[CrossRef\]](#)
11. Welch, M.J.; Redvanly, C.S. *Handbook of Radiopharmaceuticals: Radiochemistry and Applications*; John Wiley & Sons: Hoboken, NJ, USA, 2003; ISBN 978-0-470-84638-4.
12. Abram, U.; Alberto, R. Technetium and rhenium: Coordination chemistry and nuclear medical applications. *J. Braz. Chem. Soc.* **2006**, *17*, 1486–1500. [\[CrossRef\]](#)
13. Liu, S. The role of coordination chemistry in the development of target-specific radiopharmaceuticals. *Chem. Soc. Rev.* **2004**, *33*, 445–461. [\[CrossRef\]](#)
14. Maruk, A.Y.; Bruskin, A.B.; Kodina, G.E. Novel  $^{99m}Tc$  radiopharmaceuticals with bifunctional chelating agents. *Radiochemistry* **2011**, *53*, 341–353. [\[CrossRef\]](#)
15. Günther, T.; Konrad, M.; Stopper, L.; Kunert, J.P.; Fischer, S.; Beck, R.; Casini, A.; Wester, H.J. Optimization of the Pharmacokinetic Profile of  $[^{99m}Tc]Tc-N_4$ -Bombesin Derivatives by Modification of the Pharmacophoric Gln-Trp Sequence. *Pharmaceuticals* **2022**, *15*, 1133. [\[CrossRef\]](#)

16. Volkov, M.A.; Novikov, A.P.; Grigoriev, M.S.; Fedoseev, A.M.; German, K.E. Novel Synthesis Methods of New Imidazole-Containing Coordination Compounds Tc(IV, V, VII)—Reaction Mechanism, Xrd and Hirshfeld Surface Analysis. *Int. J. Mol. Sci.* **2022**, *23*, 9461. [[CrossRef](#)]
17. Sergienko, V.S.; Churakov, A.V. Specific features of technetium mononuclear octahedral oxo complexes: A review. *Crystallogr. Rep.* **2013**, *58*, 1–25. [[CrossRef](#)]
18. Kastner, M.E.; Lindsay, M.J.; Clarke, M.J. Synthesis and Structure of trans-[O<sub>2</sub>(en)<sub>2</sub>Tcv]<sup>+</sup>. *Inorg. Chem.* **1982**, *21*, 2037–2040. [[CrossRef](#)]
19. Zuckman, S.A.; Freeman, G.M.; Troutner, D.E.; Volkert, W.A.; Holmes, R.A.; Van Derveer, D.G.; Barefield, E.K. Preparation and X-ray Structure of trans-Dioxo(1,4,8,11-tetraazacyclotetradecane)technetium(V) Perchlorate Hydrate. *Inorg. Chem.* **1981**, *20*, 2386–2389. [[CrossRef](#)]
20. Nguyen, H.H.; Trieu, T.N.; Abram, U. Syntheses and Structures of Nitridorhenium(V) and Nitridotechnetium(V) Complexes with N,N'-(Dialkylamino)(thiocarbonyl)-N'-(2-hydroxyphenyl)benzamidines. *Z. Anorg. Allg. Chem.* **2011**, *637*, 1330–1333. [[CrossRef](#)]
21. Clarke, M.J.; Lu, J. Synthesis and Spectra of Cis-[NCl(phen)2Tc]Cl·H<sub>2</sub>O and c/s-[NCl(phen)2Tc]PF<sub>6</sub> and Considerations of their Structural Distortions. *Inorg. Chem.* **1992**, *31*, 2476–2480. [[CrossRef](#)]
22. Rue, K.L.; McLachlan, J.R.; Cazzaniga, J.A.; Chakraborty, I.; Dares, C.J.; Raptis, R.G. Redox-active dinuclear oxorhenium(V) pyrazolate complexes. *Inorg. Chim. Acta* **2021**, *516*, 120126. [[CrossRef](#)]
23. MacHura, B.; Dzięgielewski, J.O.; Kruszynski, R.; Bartczak, T.J.; Kusz, J. Linear and bent oxo-bridged dinuclear rhenium(V) complexes with terminal and bridging pyrazole ligands. *Inorg. Chim. Acta* **2004**, *357*, 1011–1022. [[CrossRef](#)]
24. Machura, B.; Kruszynski, R.; Jaworska, M.; Lodowski, P. Synthesis, spectroscopic characterization, crystal, molecular and electronic structure of the [{ReOBr<sub>2</sub>(pyz)<sub>2</sub>}(μ-O)] and [{ReOBr<sub>2</sub>}(μ-O)(μ-pyd)<sub>2</sub>] complexes. *Polyhedron* **2005**, *24*, 1893–1906. [[CrossRef](#)]
25. Machura, B.; Kruszynski, R.; Kusz, J. Reactivity of [ReOX<sub>3</sub>(PPh<sub>3</sub>)<sub>2</sub>] complexes towards pyridazine. X-ray structures of [{ReOCl<sub>2</sub>}(μ-O)(μ-pyd)<sub>2</sub>]-C<sub>6</sub>H<sub>6</sub> and [{ReOBr<sub>2</sub>}(μ-O)(μ-pyd)<sub>2</sub>]-CH<sub>3</sub>CN, and DFT calculations for [{ReOCl<sub>2</sub>}(μ-O)(μ-pyd)<sub>2</sub>]. *Polyhedron* **2007**, *26*, 3054–3062. [[CrossRef](#)]
26. Machura, B.; Wolff, M.; Palion, J.; Benoist, E. Synthesis, spectroscopic characterization and X-ray crystal structures of mononuclear and binuclear oxidorhenium(V) complexes containing indazolyl moieties. *Inorg. Chim. Acta* **2013**, *404*, 144–154. [[CrossRef](#)]
27. Fackler, P.H.; Kastner, M.E.; Clarke, M.J. Synthesis, spectra, and structure of af-dibromo-b-ethoxo-d-oxo-ce-bis(4-nitropyridine) technetium(V) and related. *Inorg. Chem.* **1984**, *23*, 3968–3972. [[CrossRef](#)]
28. Lock, C.J.L.; Turner, G. Studies of the rhenium-oxygen bond. III. The crystal and molecular structure of 1-oxo-6-ethoxo-2,4-dichloro-3,5-dipyridinerhenium(V). *Can. J. Chem.* **1972**, *55*, 333–339. [[CrossRef](#)]
29. Fortin, S.; Beauchamp, A.L. Synthesis and crystal structure of a new isomer of the μ-oxo-bis[dichlorooxobis(pyridine)rhenium(V)] complex {OReCl<sub>2</sub>py<sub>2</sub>}<sub>2</sub>O. *Inorg. Chim. Acta* **1998**, *279*, 159–164. [[CrossRef](#)]
30. Iengo, E.; Zangrando, E.; Mestroni, S.; Fronzoni, G.; Stener, M.; Alessio, E. Complexed bridging ligands: Oxorhenium(V) compounds with mono-coordinated pyrazine or pyrimidine as possible building blocks for the construction of polynuclear architectures. *J. Chem. Soc. Dalton Trans.* **2001**, 1338–1346. [[CrossRef](#)]
31. Daolio, A.; Pizzi, A.; Terraneo, G.; Frontera, A.; Resnati, G. Anion·Anion Interactions Involving σ-Holes of Perrhenate, Pertechnetate and Permanganate Anions. *ChemPhysChem* **2021**, *22*, 2281–2285. [[CrossRef](#)]
32. Novikov, A.P.; German, K.E.; Safonov, A.V.; Grigoriev, M.S. Cation Protonation Degree Influence on the Formation of Anion···Anion and Other Non-Valent Interactions in Guaninium Perrhenates and Pertechnetate. *ChemistrySelect* **2022**, *7*, e202202814. [[CrossRef](#)]
33. Xie, R.; Shen, N.; Chen, X.; Li, J.; Wang, Y.; Zhang, C.; Xiao, C.; Chai, Z.; Wang, S. <sup>99</sup>TcO<sub>4</sub>-Separation through Selective Crystallization Assisted by Polydentate Benzene-Aminoguanidinium Ligands. *Inorg. Chem.* **2021**, *60*, 6463–6471. [[CrossRef](#)]
34. Zhu, L.; Sheng, D.; Xu, C.; Dai, X.; Silver, M.A.; Li, J.; Li, P.; Wang, Y.; Wang, Y.; Chen, L.; et al. Identifying the Recognition Site for Selective Trapping of <sup>99</sup>TcO<sub>4</sub>- in a Hydrolytically Stable and Radiation Resistant Cationic Metal-Organic Framework. *J. Am. Chem. Soc.* **2017**, *139*, 14873–14876. [[CrossRef](#)] [[PubMed](#)]
35. Zhu, L.; Xiao, C.; Dai, X.; Li, J.; Gui, D.; Sheng, D.; Chen, L.; Zhou, R.; Chai, Z.; Albrecht-Schmitt, T.E.; et al. Exceptional perrhenate/pertechnetate uptake and subsequent immobilization by a low-dimensional cationic coordination polymer: Overcoming the hofmeister bias selectivity. *Environ. Sci. Technol. Lett.* **2017**, *4*, 316–322. [[CrossRef](#)]
36. Sheng, D.; Zhu, L.; Dai, X.; Xu, C.; Li, P.; Pearce, C.I.; Xiao, C.; Chen, J.; Zhou, R.; Duan, T.; et al. Successful Decontamination of <sup>99</sup>TcO<sub>4</sub>- in Groundwater at Legacy Nuclear Sites by a Cationic Metal-Organic Framework with Hydrophobic Pockets. *Angew. Chem.* **2019**, *131*, 5022–5026. [[CrossRef](#)]
37. Artemjev, A.A.; Novikov, A.P.; Burkin, G.M.; Sapronov, A.A.; Kubasov, A.S.; Nenajdenko, V.G.; Khrustalev, V.N.; Borisov, A.V.; Kirichuk, A.A.; Kritchenkov, A.S.; et al. Towards Anion Recognition and Precipitation with Water-Soluble 1,2,4-Selenodiazolium Salts: Combined Structural and Theoretical Study. *Int. J. Mol. Sci.* **2022**, *23*, 6372. [[CrossRef](#)] [[PubMed](#)]
38. Chotkowski, M.; Wrzosek, B.; Grdeń, M. Intermediate oxidation states of technetium in concentrated sulfuric acid solutions. *J. Electroanal. Chem.* **2018**, *814*, 83–90. [[CrossRef](#)]
39. Li, J.; Li, B.; Shen, N.; Chen, L.; Guo, Q.; Chen, L.; He, L.; Dai, X.; Chai, Z.; Wang, S. Task-Specific Tailored Cationic Polymeric Network with High Base-Resistance for Unprecedented <sup>99</sup>TcO<sub>4</sub>-Cleanup from Alkaline Nuclear Waste. *ACS Cent. Sci.* **2021**, *7*, 1441–1450. [[CrossRef](#)]

40. Machura, B.; Kruszynski, R.; Kusz, J. A novel oxo-bridged rhenium complex with Re centers in different coordination environments—Synthesis, spectroscopic characterization and X-ray structure. *Inorg. Chem. Commun.* **2007**, *10*, 494–497. [[CrossRef](#)]
41. Pervukhina, N.V.; Sokolov, M.N.; Fedorova, N.; Fedorov, V.E. Crystal Structures of Two Re(V) Complexes of 3,5-Dimethylpyrazole with Linear and Bent [OReOREO]<sub>4</sub><sup>+</sup> Fragments. *J. Struct. Chem.* **2001**, *42*, 833–837. [[CrossRef](#)]
42. Kückmann, T.I.; Abram, U. Oxorhenium(V)- and Tricarbonylrhenium(I) Complexes with Substituted Pyrazoles as Products of the Degradation of Hydrotrispyrazolylborates. *Z. Anorg. Allg. Chem.* **2004**, *630*, 783–785. [[CrossRef](#)]
43. Sokolov, M.N.; Fedorova, N.E.; Pervukhina, N.V.; Peresypkina, E.V.; Virovets, A.V.; Pätow, R.; Fedorov, V.E.; Fenske, D. Rhenium(IV) and rhenium(V) complexes with 3,5-dimethylpyrazole. *Russ. Chem. Bull.* **2006**, *55*, 53–61. [[CrossRef](#)]
44. Novikov, A.P.; Volkov, M.A.; Safonov, A.V.; Grigoriev, M.S. Synthesis, Crystal Structure, and Hirshfeld Surface Analysis of Hexachloroplatinate and Tetraclorouranilate of 3-Carboxypyridinium—Halogen Bonds and  $\pi$ -Interactions vs. Hydrogen Bonds. *Crystals* **2022**, *12*, 271. [[CrossRef](#)]
45. Alvarez, S. A cartography of the van der Waals territories. *Dalt. Trans.* **2013**, *42*, 8617–8636. [[CrossRef](#)] [[PubMed](#)]
46. Spiwok, V. CH/ $\pi$  Interactions in Carbohydrate Recognition. *Molecules* **2017**, *22*, 1038. [[CrossRef](#)] [[PubMed](#)]
47. Wang, L.; Hao, J.; Zhai, L.X.; Zhang, Y.; Dong, W.K. Synthesis, Crystal Structure, Luminescence, Electrochemical and Antimicrobial Properties of Bis(salamo)-Based Co(II) Complex. *Crystals* **2017**, *7*, 277. [[CrossRef](#)]
48. Nishio, M. The CH/ $\pi$  hydrogen bond in chemistry. Conformation, supramolecules, optical resolution and interactions involving carbohydrates. *Phys. Chem. Chem. Phys.* **2011**, *13*, 13873–13900. [[CrossRef](#)]
49. Nishio, M. CH/ $\pi$  hydrogen bonds in organic reactions. *Tetrahedron* **2005**, *61*, 6923–6950. [[CrossRef](#)]
50. Zhuo, H.; Li, Q.; Li, W.; Cheng, J. Is  $\pi$  halogen bonding or lone pair  $\cdots \pi$  interaction formed between borazine and some halogenated compounds? *Phys. Chem. Chem. Phys.* **2013**, *16*, 159–165. [[CrossRef](#)]
51. Shah, M.B.; Liu, J.; Zhang, Q.; Stout, C.D.; Halpert, J.R. Halogen- $\pi$  Interactions in the Cytochrome P450 Active Site: Structural Insights into Human CYP2B6 Substrate Selectivity. *ACS Chem. Biol.* **2017**, *12*, 1210. [[CrossRef](#)]
52. Mitra, D.; Bankoti, N.; Michael, D.; Sekar, K.; Row, T.N.G. C-halogen  $\cdots \pi$  interactions in nucleic acids: A database study. *J. Chem. Sci.* **2020**, *132*, 93. [[CrossRef](#)]
53. Riley, K.E.; Tran, K.A. Strength and Character of R-X  $\cdots \pi$  Interactions Involving Aromatic Amino Acid Sidechains in Protein-Ligand Complexes Derived from Crystal Structures in the Protein Data Bank. *Crystals* **2017**, *7*, 273. [[CrossRef](#)]
54. Dumitrescu, D.; Shova, S.; Man, I.C.; Caira, M.R.; Popa, M.M.; Dumitrascu, F. 5-Iodo-1-Arylpyrazoles as Potential Benchmarks for Investigating the Tuning of the Halogen Bonding. *Crystals* **2020**, *10*, 1149. [[CrossRef](#)]
55. Novikov, A.P.; Volkov, M.A.; Safonov, A.V.; Grigoriev, M.S.; Abkhalimov, E.V. Synthesis and Characterization of New Guanine Complexes of Pt(IV) and Pd(II) by X-Ray Diffraction and Hirshfeld Surface Analysis. *Crystals* **2021**, *11*, 1417. [[CrossRef](#)]
56. Spackman, M.A.; Jayatilaka, D. Hirshfeld surface analysis. *CrystEngComm* **2009**, *11*, 19–32. [[CrossRef](#)]
57. Scheiner, S. *Noncovalent Forces*; Springer International Publishing: Berlin/Heidelberg, Germany, 2015; ISBN 9783319141633.
58. Psycharis, V.; Dermizaki, D.; Raptopoulou, C.P. The Use of Hirshfeld Surface Analysis Tools to Study the Intermolecular Interactions in Single Molecule Magnets. *Crystals* **2021**, *11*, 1246. [[CrossRef](#)]
59. Liu, M.; Yin, C.; Chen, P.; Zhang, M.; Parkin, S.; Zhou, P.; Li, T.; Yu, F.; Long, S. sp<sup>2</sup>CH  $\cdots$  Cl hydrogen bond in the conformational polymorphism of 4-chloro-phenylanthranilic acid. *CrystEngComm* **2017**, *19*, 4345–4354. [[CrossRef](#)]
60. Marek, P.H.; Urban, M.; Madura, I.D. The study of interactions with a halogen atom: Influence of NH<sub>2</sub> group insertion on the crystal structures of meta-bromonitrobenzene derivatives. *Acta Crystallogr. Sect. C Struct. Chem.* **2018**, *74*, 1509–1517. [[CrossRef](#)]
61. Novikov, A.P.; Bezdornikov, A.A.; Grigoriev, M.S.; German, K.E. Synthesis, crystal structure and Hirshfeld surface analysis of 2-(perfluorophenyl)acetamide in comparison with some related compounds. *Acta Crystallogr. Sect. E Crystallogr. Commun.* **2022**, *78*, 80–83. [[CrossRef](#)]
62. Spackman, P.R.; Turner, M.J.; McKinnon, J.J.; Wolff, S.K.; Grimwood, D.J.; Jayatilaka, D.; Spackman, M.A. CrystalExplorer: A program for Hirshfeld surface analysis, visualization and quantitative analysis of molecular crystals. *J. Appl. Crystallogr.* **2021**, *54*, 1006–1011. [[CrossRef](#)]
63. Groom, C.R.; Bruno, I.J.; Lightfoot, M.P.; Ward, S.C. The Cambridge Structural Database. *Acta Crystallogr. Sect. B Struct. Sci. Cryst. Eng. Mater.* **2016**, *72*, 171–179. [[CrossRef](#)] [[PubMed](#)]
64. Dirghangi, B.K.; Menon, M.; Pramanik, A.; Chakravorty, A. A Triad of Variable-Valent Rhenium Aldimine and Amide Systems Interrelated by Successive Oxygen Atom Transfer. *Inorg. Chem.* **1997**, *36*, 1095–1101. [[CrossRef](#)] [[PubMed](#)]
65. Lahiri, G.K.; Goswami, S.; Falvello, L.R.; Chakravorty, A. A New Family of Semibent Rhenium(V) Arylimides Formed by Azo Splitting: Structure, Bonding, and Electrooxidation to Rhenium(VI) Congeners. *Inorg. Chem.* **1987**, *26*, 3365–3370. [[CrossRef](#)]
66. Du Preez, J.G.H.; Gerber, T.I.A.; Fourie, P.J.; Van Wyk, A.J. The Chemistry of rhenium and technetium. Part 1. Syntheses and characterisation of new dioxo technetium(V) complexes with schiff base type ligands. *Inorg. Chim. Acta* **1984**, *82*, 201–205. [[CrossRef](#)]
67. L'Annunziata, M.F. (Ed.) *Handbook of Radioactivity Analysis: Volume 2. Radioanalytical Applications*; Academic Press: Cambridge, MA, USA, 2020; ISBN 978-0-12-814395-7.
68. Bruker AXS Inc.: Madison, WI, USA. *SAINT, V8.40B*, Elsevier: Edinburgh, UK, 2020.
69. Krause, L.; Herbst-Irmer, R.; Sheldrick, G.M.; Stalke, D. Comparison of silver and molybdenum microfocus X-ray sources for single-crystal structure determination. *J. Appl. Crystallogr.* **2015**, *48*, 3–10. [[CrossRef](#)]

70. Sheldrick, G.M. SHELXT-Integrated space-group and crystal-structure determination. *Acta Crystallogr. Sect. A Found. Crystallogr.* **2015**, *71*, 3–8. [[CrossRef](#)]
71. Sheldrick, G.M. Crystal structure refinement with SHELXL. *Acta Crystallogr. Sect. C Struct. Chem.* **2015**, *71*, 3–8. [[CrossRef](#)]
72. Dolomanov, O.V.; Bourhis, L.J.; Gildea, R.J.; Howard, J.A.K.; Puschmann, H. OLEX2: A complete structure solution, refinement and analysis program. *J. Appl. Crystallogr.* **2009**, *42*, 339–341. [[CrossRef](#)]